

RESEARCH ARTICLE OPEN ACCESS

## Denaturation of Water in Alkaline Melts

Xudong Zhang<sup>1</sup> | Oldamur Hollóczki<sup>2</sup> | Johannes Ingenmey<sup>3</sup> | Barbara Kirchner<sup>3</sup> | Michael Ruck<sup>1</sup><sup>1</sup>Faculty of Chemistry and Food Chemistry, TUD Dresden University of Technology, Dresden, Germany | <sup>2</sup>Faculty of Science and Technology, Department of Physical Chemistry, University of Debrecen, Debrecen, Hungary | <sup>3</sup>Mulliken Center for Theoretical Chemistry, University of Bonn, Bonn, Germany**Correspondence:** Oldamur Hollóczki ([holloczki.oldamur@science.unideb.hu](mailto:holloczki.oldamur@science.unideb.hu)) | Barbara Kirchner ([bkirch@uni-bonn.de](mailto:bkirch@uni-bonn.de)) | Michael Ruck ([michael.ruck@tu-dresden.de](mailto:michael.ruck@tu-dresden.de))**Received:** 25 August 2025 | **Revised:** 21 November 2025 | **Accepted:** 25 November 2025**Keywords:** ab initio molecular-dynamics simulation | alkali | hydroflux | vapor pressure | water

## ABSTRACT

Extremely high base concentrations ( $c_B$ ) in ultra-alkaline liquids, also known as hydroflux, alter the thermodynamic and structural properties of water. Mixtures of water and alkali (AOH,  $A = \text{Na, K}$ ) with molar base ratios of  $q(A) = n(\text{H}_2\text{O}):n(\text{AOH}) \leq 2:1$  ( $c_B \geq 25 \text{ mol L}^{-1}$ ) show an overproportionally reduced vapor pressure compared to more diluted systems. The vapor pressure of a melt with  $q(A) = 0.8$  ( $c_B = 70 \text{ mol L}^{-1}$ ) at  $200^\circ\text{C}$  is negligible. Ab initio molecular dynamics simulations revealed substantial structural reorganization of the hydrogen bonding network in the equimolar mixture of KOH and water. Distinctive molecular features included altered coordination geometries, shortened hydrogen bonds, and frequent proton transfer events, including Grotthuss diffusion, indicative of an altered hydrogen-bond network and increased proton mobility. Cluster population analysis shows that a significant number of  $\text{H}_3\text{O}_2^-$  anions are present, which exhibit a near symmetrical hydrogen bond with  $\text{O}\cdots\text{H}$  distances  $<1.28 \text{ \AA}$ . The hydroflux can be seen as an intermediate between an alkaline solution and a molten salt  $\{\text{K}^+\cdot\text{H}^+\cdot 2\text{OH}^-\}$ , in which the water has a vanishing chemical activity.

## 1 | Introduction

To increase the sustainability of chemical industries, alternative reaction pathways are being sought that require less energy, are more atomically efficient, and produce less waste overall. New approaches include chemical reactions using the hydroflux method. A hydroflux medium can be considered a highly concentrated aqueous electrolyte solution or the melt of a wet salt. Typical molar ratios of water to salt  $q(A) = n(\text{H}_2\text{O}):n(\text{AOH})$  are in the range from 0.8 to 2, which corresponds to solutions with base concentrations  $70 \leq c_B \leq 25 \text{ mol L}^{-1}$  (molar, M). The addition of water to salts lowers the melting point. For example, pure KOH melts at  $360^\circ\text{C}$ ,  $\text{KOH}\cdot\text{H}_2\text{O}$  at  $127^\circ\text{C}$ .<sup>[1]</sup> Syntheses in a hydroflux medium are characterized by moderate temperatures of up to  $240^\circ\text{C}$  (limited by the autoclave material) and short reaction times (often less than one day). Typically, the products are single-phase, well crystallized, and obtained in high yields.

This approach enables the synthesis of known substances with greater efficiency compared to conventional methods but, also facilitates the discovery of new compounds. The term “hydroflux” has been coined in 1975 by *Elwell* and *Scheel*, who also suggested using hydroflux as a reaction medium.<sup>[2]</sup> This was however only done once by *Harms* and *Gunßer* in 1986, who employed a hydroflux medium based on  $\text{NaNO}_3$  and  $\text{KNO}_3$  to synthesize gallium oxides.<sup>[3]</sup> In the last decade, first *zur Loye* <sup>[4–8]</sup> and then we <sup>[9–13]</sup> took up this idea again and applied it to synthesize a wide variety of oxometalates in highly concentrated alkaline media. Lately, the method has attracted increasing scientific attention.<sup>[14–17]</sup>

In the course of these investigations, it became clear that alkaline hydroflux is a unique reaction medium. Firstly, the vapor pressure appeared to be much lower than in more water-rich solutions, which are used in, for instance, hydrothermal synthesis.<sup>[4, 6]</sup>

This is an open access article under the terms of the [Creative Commons Attribution](https://creativecommons.org/licenses/by/4.0/) License, which permits use, distribution and reproduction in any medium, provided the original work is properly cited.

© 2025 The Author(s). *Chemistry – A European Journal* published by Wiley-VCH GmbH.

Secondly, despite the aqueous solvent system, highly hygroscopic compounds were also possible to obtain.[11] Thirdly, the ultra-alkaline medium is far from standard conditions, so the tabulated electrochemical potentials do not apply, resulting in unexpected redox chemistry.[11, 13]

Since the unique physicochemical features of hydroflux media should be the key to their efficiency and to obtain peculiar materials in the syntheses performed in them, understanding and characterizing the properties of these solvents is essential to their further development, and to achieve their full potential. Although the behavior of electrolytes and alkaline solutions is textbook chemistry, knowledge becomes scarcer when approaching toward high concentrations, and therefore, further in-depth studies are necessary in this field.

The lack of information is especially apparent for molecular-level theoretical studies, which so far have focused on less concentrated systems. Besides the influence of the electronic structure theory and the effect of nuclear quantum effects,[18, 19] the state of the hydronium [20] or hydroxide ions [18, 21] in water is highly debated, even regarding the better investigated systems, and no final arguments seem to have been made. For the hydronium ion, several schools of thought are present, including the idea of the Zundel ion  $\text{H}_5\text{O}_2^+$  and the Eigen ion  $\text{H}_9\text{O}_4^+$ , with a proton equally shared between two water molecules in the former and a  $\text{H}_3\text{O}^+$  ion surrounded by three water molecules in the latter case.[20] Whereas *Voth* shows strong arguments in favor of the solvation of the hydronium ion as a distorted Eigen ion,[22] some studies suggest a mixture of these two, in which one hydronium ion and one of the three water molecules transiently become a Zundel-like structure within the Eigen ion as a special pair dance.[18, 20] *Hassanali* highlighted another aspect, namely, for the recombination of hydronium separated by two water molecules from the hydroxide, a compressed wire effect comes into play, making all involved (hydrogen) bonds shorter than in the normal water system.[23]

For the solvated hydroxide ion, a tetrahedral (accepting three hydrogen bonds and donating one) and a hypercoordinated (accepting four hydrogen bonds and donating none) solvation mode have been shown to be present.[18] Both the solvated hydronium and tetrahedral hydroxide ions can rearrange in aqueous solutions via proton transfers to or from the surrounding water molecules. Through these proton transfer events, the charge can diffuse faster in solution than the actual atoms, which is referred to as structural or Grotthuss-type diffusion [24] in the literature. Although the charge diffuses in both systems (i.e., in either acidic or basic media), hydroxide ions can, interestingly, contribute to conductivities remarkably less than hydronium ions. The reason for this remarkable discrepancy was suggested to be the high stability of the hypercoordinated hydroxide ion, which can, therefore, be considered a resting state of the structural diffusion.[18]

In light of the aforementioned various aspects of ion solvation and Grotthuss diffusion, the question is apparent: what kind of molecular structure and dynamics arise from these solvation modes and diffusion mechanisms in highly concentrated alkaline solutions? It is very likely that the unusual reactions that occur in hydroflux media are due to unique behavior at the molecular

level, and therefore, understanding it in detail is crucial. This prompted us to investigate the reduced chemical activity of water in alkaline hydroflux media more thoroughly. The highly aggressive nature of the ultra-alkaline medium, which increases when heated, requires a reaction vessel that does not allow optical or spectroscopic examination with simple means. We therefore performed vapor pressure measurements in a polytetrafluoroethylene (PTFE) lined autoclave as well as ab initio molecular-dynamics simulations (AIMD). Together with the earlier experimental results and the compounds crystallized from alkaline hydroflux in recent years, a coherent picture emerges.

## 2 | Results and Discussion

### 2.1 | Vapor Pressure

The pressure in a PTFE-lined steel autoclave equipped with an automated manometer (Figure S1 of the Supporting Information) was monitored (Figure S2) for different base concentrations  $q(A) = n(\text{H}_2\text{O}):n(\text{AOH})$  for  $A = \text{Na}, \text{K}$  between room temperature and 200 °C. For this purpose, solid NaOH or KOH and water were filled into the autoclave under ambient conditions. The heating time to 200 °C was set to 16 h, which corresponds to a rate of slightly less than 0.5 K min<sup>-1</sup>. The autoclave was kept at 200 °C for 6 h and then cooled to room temperature within 2 h.

The manufacturer specifies an accuracy of 1 K for the temperature sensor and 2 bar for the pressure sensor, which can measure up to 200 bar. To check for nonequilibrium effects in the first heating cycle, the experiment was repeated after 30 min using the same heating rate. We found that the  $p/T$  data for subsequent heating curves agree within experimental accuracy (Figure S3 and S7, Table S2), indicating that equilibrium was established during the measurement. Even at the highest base concentrations, we found no residues of solid NaOH or KOH after the measurements, so that the composition of the molten hydroflux medium should correspond to the ratio of the starting materials. Consequently, the (unknown) melting point of the mixtures with very high alkali content must also lie below 200 °C in all cases.

Figure 1 and Table 1 show the temperature-dependent evolution of the measured total pressure in the autoclave for mixtures of alkali AOH ( $A = \text{Na}, \text{K}$ ) and water with various concentrations. Up to the highest concentration of almost 70 M, that is, a molar water-base ratio of  $q(A) = 0.8$ , the vapor pressure decreases, and the estimated boiling point increases with increasing base concentration. The same observation has been made earlier for NaOH and KOH solutions with concentrations up to 25 and 18 M, respectively.[25] For  $q(A) \leq 1$ , which nominally corresponds to a concentration of  $\geq 55.6$  M, a vapor pressure exceeding 1 bar is observed only close to or above 200 °C. This confirms previous reports of a remarkably low vapor pressure that develops during hydroflux syntheses. [4, 6] It also resembles the behavior of ionic liquids.[26]

For the samples with base concentrations  $c_B \geq 30$  M, a slight decrease of the total pressure is observed upon heating (Figure 1). This is unexpected, since at least the increase in the gas pressure of the enclosed air should be seen. A reduction of the pressure below the value at room temperature can be rationalized if the

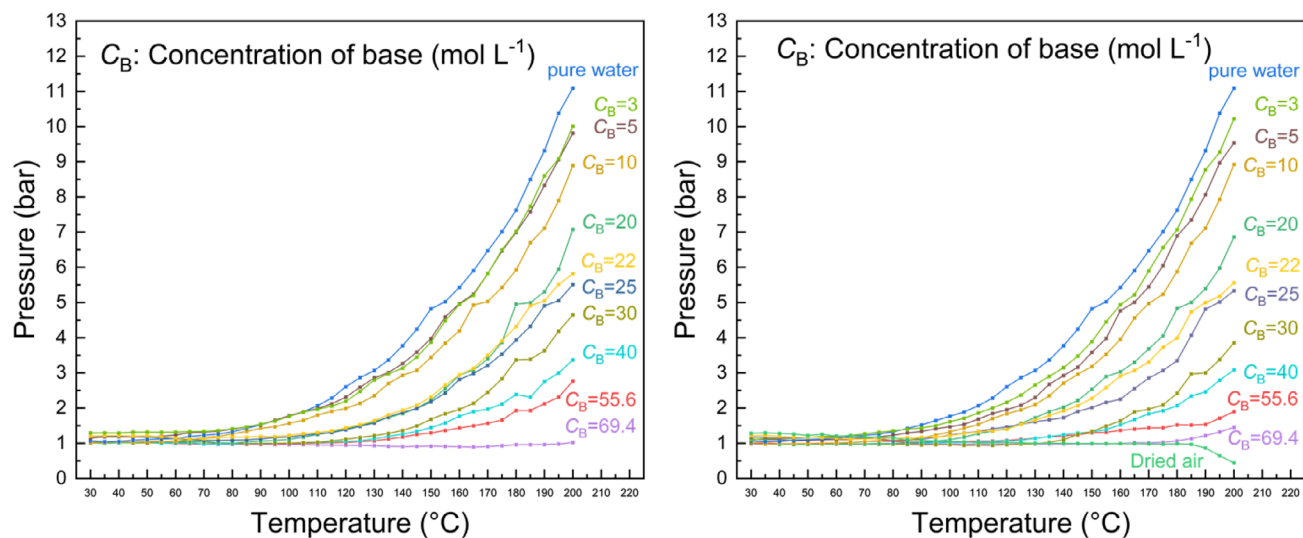


**FIGURE 1** | Total pressure developed in a PTFE-lined autoclave when heating mixtures of water and solid AOH (left:  $A = \text{Na}$ ; right:  $A = \text{K}$ ) with different base concentrations.

**TABLE 1** | Total pressure in the autoclave after heating AOH solutions with various concentrations to 150°C and 200°C. The boiling point  $T_b$  is here defined as the temperature at which the total pressure exceeds its room temperature value during heating. First value  $A = \text{Na}$ , second value in italics  $A = \text{K}$ .

$q(A)$	$c_B$ (mol L <sup>-1</sup> )	$x_{\text{H}_2\text{O}}$	$p$ (bar) at 150°C	$p$ (bar) at 200°C	$T_b$ (°C)
0.8:1	69.4	0.44	0.92 / 0.98	1.02 / 1.45	>200 / >200
1:1	55.6	0.50	1.29 / 1.29	2.77 / 1.90	187 / >200
1.39:1	40	0.58	1.44 / 1.32	3.37 / 3.09	171 / 177
1.87:1	30	0.65	1.68 / 1.33	4.65 / 3.86	161 / 171
2.23:1	25	0.69	2.17 / 2.02	5.51 / 5.04	145 / 150
2.53:1	22	0.72	2.31 / 2.28	5.81 / 5.36	142 / 143
2.78:1	20	0.74	2.22 / 2.53	7.08 / 6.86	145 / 139
5.56:1	10	0.85	3.44 / 3.18	8.89 / 8.92	120 / 127
11.1:1	5	0.92	3.98 / 3.58	9.81 / 9.53	110 / 122
18.7:1	3	0.95	3.87 / 3.88	10.01 / 10.22	112 / 115
Pure water	0	1.00	4.82	11.09	107

solution/melt has a higher density than the weighted average of the components. Additional small contributions could arise from the absorption of the  $\text{CO}_2$  content of the enclosed air and some oxygen that reacts with the alkaline medium to form superoxide and peroxide ions. The physisorption of molecular oxygen is negligible in aqueous alkaline solutions.[27] However, the observed effects, especially in the upper temperature range, are much too large to be explained in this way.

As long as there is a liquid phase, the vapor pressure should be independent of the filling level of the autoclave. Using the ideal gas law to estimate the amount of water in the gas phase suggests that there should be enough water in all experiments to ensure the presence of a liquid phase at all temperatures. However, we found an unexpected dependence of the measured pressure of pure water on the filling level, as well as negative deviations from

the theoretically expected vapor pressure of water (about 15.5 bar at 200°C [25]). Residual impurities in the “deionized” water used were not responsible for this effect, as an experiment with freshly distilled water showed (Figure S6).

Finally, a measurement with the autoclave containing only dry air did not show the expected linear increase in internal pressure with temperature. Instead, a slight decrease was found, which grew dramatically above 190°C (Figure 1, right). Such a behavior can be caused by a combination of trapped air inside the encapsulated pressure sensor, resulting in pressure compensation, and leaks in the autoclave that reduce the air pressure in the autoclave volume but not inside the pressure sensor. The leakage rate cannot be high, as the escape of hot gas to the outside was not perceptible, and the pressure built up to 11.5 bar.

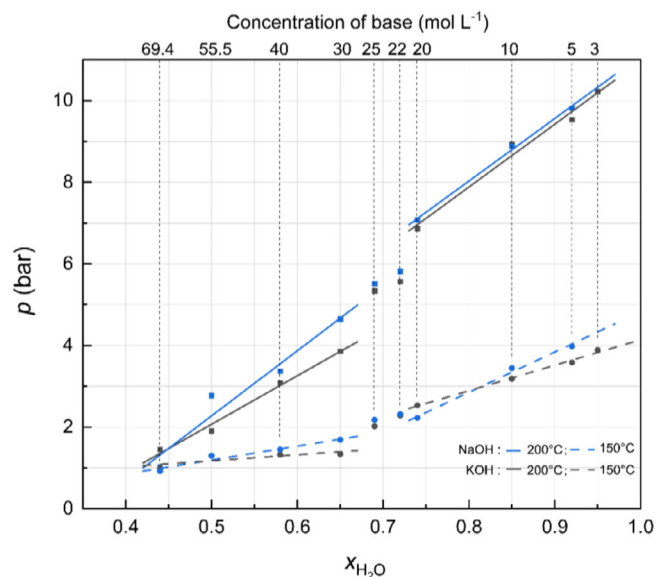


**FIGURE 2** | Relationship between the total pressure in the autoclave and the mole fraction of water in AOH solutions and melts ( $A = \text{Na}, \text{K}$ ) at 150 °C and 200 °C.

Since the pressures measured with this device cannot be regarded as correct absolute values for the total pressure, no further corrections were applied to the measured data. Nevertheless, the measurements that were carried out with the same amount of water should allow for relative comparisons. The plots of the pressure at 150 °C and 200 °C against the mole fraction of water  $x_{\text{H}_2\text{O}}$  shows two separated regimes for both alkali, each with almost linear dependency (Figure 2). In the range  $0.5 \leq x_{\text{H}_2\text{O}} \leq 0.65$ , which corresponds to the highly concentrated solutions  $55.6 \text{ M} \geq c_{\text{B}} \geq 30 \text{ M}$ , the vapor pressure of KOH solutions is 1 to 2 bar lower than would be expected from a linear extrapolation of the range of the less concentrated solutions with  $x_{\text{H}_2\text{O}} \geq 0.74$ , that is,  $c_{\text{B}} \leq 20 \text{ M}$ . The difference between the two regimes is more pronounced for KOH than for NaOH. In between the two regimes lies the base concentration  $c_{\text{B}} = 25 \text{ mol L}^{-1}$ . Therefore, we suggest using this value to distinguish between hydroflux and hydrothermal conditions in aqueous alkaline media.

The corresponding molar water-base ratio of about  $q(A) = 2$  translates this threshold concentration into a molecular picture: The special properties of alkaline hydroflux occur when there is no more than one water molecule per ion. To rationalize these observations, it is necessary to understand the structure and intermolecular interactions within the system and the difference from a dilute aqueous solution. The typical coordination of a potassium cation, as observed in crystals, involves six water molecules or hydroxide ions.  $[\text{K}(\text{OH})(\text{H}_2\text{O})_5]$  groups without additional free water molecules are nominally obtained at  $q(\text{K}) = 5$ . A higher base concentration results in condensation of these complexes with bridging water and hydroxide ligands. In agreement,  $\text{K}^+$  cations in solid  $\text{KOH} \cdot \text{H}_2\text{O}$ , which could be seen as a crystallized hydroflux with  $q(\text{K}) = 1$ , have octahedral coordination (Figure 3) and every oxygen atom coordinates on average three  $\text{K}^+$  cations.<sup>[1]</sup> Such strongly bonded water molecules develop a very low vapor pressure. On the other hand, the water molecules reduce

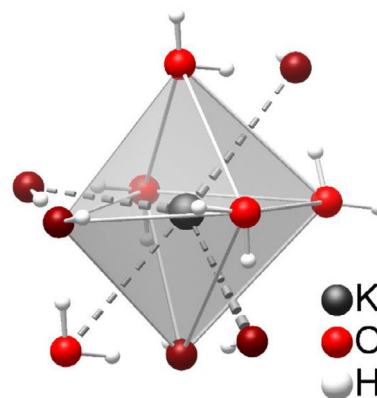


**FIGURE 3** | [6+4]-coordination of the  $\text{K}^+$  cation in solid  $\text{KOH} \cdot \text{H}_2\text{O}$ . The light red colored oxygen atoms belong to the water molecules, the dark red colored ones to the hydroxide ions. K–O distances in the distorted octahedron range from 279 to 294 pm, the dotted connections range from 327 to 362 pm. The distances to the next two O atoms (not shown) are 429 and 432 pm, which exceed the distance to the next  $\text{K}^+$  cation (394 pm).

the electrostatic interactions between  $\text{K}^+$  and  $\text{OH}^-$  ions, thus lowering the melting point compared to anhydrous KOH.

## 2.2 | Ab Initio Molecular-Dynamics Simulations

To understand the molecular-level effects that lead to the aforementioned properties of hydroflux media, we performed *ab initio* molecular dynamics simulations on a system containing 150  $\text{H}_2\text{O}$  molecules and 150  $\text{K}^+$  cations and  $\text{OH}^-$  anions, corresponding to  $q(\text{K}) = 1$  or  $c_{\text{B}} = 55.6 \text{ M}$ . For the simulation details, see the Supporting Information. The visual inspection of the trajectory showed that within the 50-ps physical time of the simulation, numerous proton transfer processes occurred, suggesting that this system is highly dynamic. This finding is in clear contrast with earlier studies for dilute systems, in which such proton transfers were found significantly rarer. To support this observation with quantitative data, the structure and dynamics of the system were analyzed in detail.

As described in the introduction, the solvation of dilute aqueous  $\text{OH}^-(\text{aq})$  alternates between two states.<sup>[18]</sup> On one hand, a hypercoordinated structure is present with four water hydrogen atoms coordinating to the oxygen atom of hydroxide, while no hydrogen bond is being donated. On the other hand, a tetrahedral configuration forms with up to three water hydrogen atoms coordinating to the oxygen atom of the anion, and water oxygen atom to its hydrogen atom. This is in stark contrast to our hydroflux system, where we find on average less than two (1.8) water molecules donating a hydrogen bond to the hydroxide anion, with an occasional hydrogen bond donation from the hydroxide to a water molecule (17.7% of the time). Under closer scrutiny, the most often occurring number of hydrogen bonds accepted by a single hydroxide from water molecules is also 2 (43.9%), but single (39.8%) and threefold coordination modes (10.8%) also occur, albeit with much lower probability. The aforementioned hypercoordinated system is very rarely observed in the simulation, on average only 0.6% of the time for a single hydroxide. Unlike an ideal Zundel ion for the hydronium ion (described in

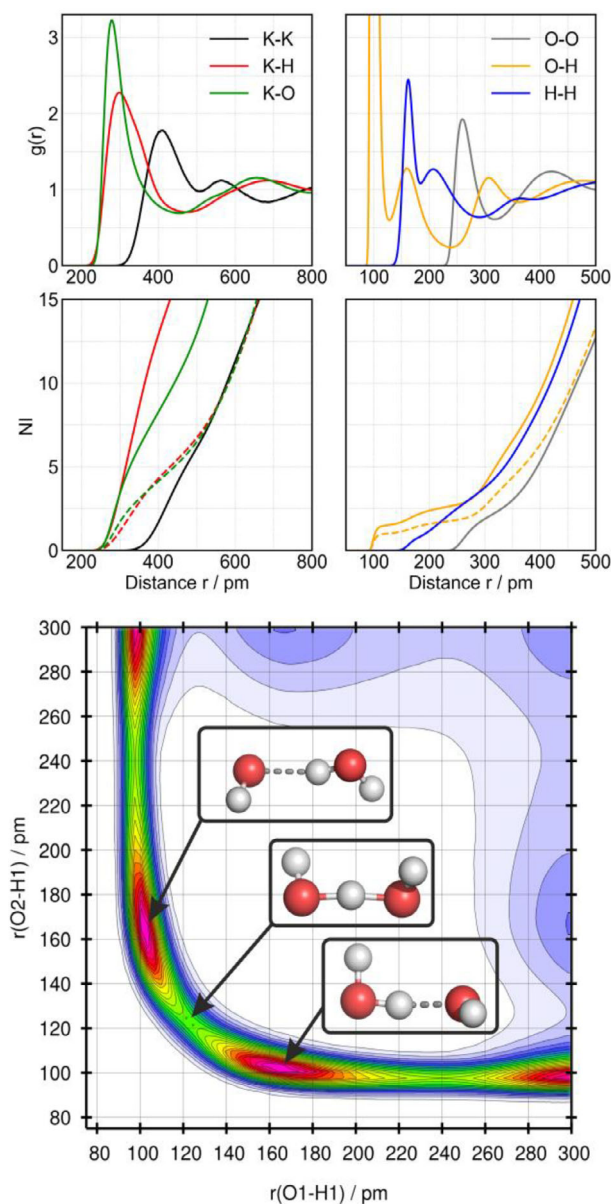


**FIGURE 4** | Upper panel: Radial distribution function (above) and number integral (below) of left: K atom with K (black), H (red), and O (green) atoms; and right: O atom with O (dark grey), H (orange), and H with H (blue) atoms. Note the x-axis is different on the left than on the right. The dotted lines are the reversed coordination in the case of mixed atom functions. Lower panel: Combined distribution function of two O-H RDFs, including ball-and-stick representation of structures out of the simulation. Please note that they are further (hydrogen) bonded and do not occur as isolated entities.

the introduction), the hydrogen bonding interplay between the hydroxide ion and the water molecule is clearly asymmetric, with a strong difference between a more covalent O-H bond within the water molecule, and a less covalent intermolecular hydrogen bond. This is obviously visible from the O-H radial distribution function (RDF), showing a minimum [and not a maximum] at this distance (at 128 pm, Figure 4 top right, orange). In the course of a proton transfer, however, a transient quasi-symmetrical structure as previously experimentally observed [28] occurs with an average lifetime of about 0.2 ps (Figure 4 lower panel). As

**TABLE 2** | Location of the maximum/minimum  $g(r)$  distance ( $r_{\max}/r_{\min}$ ) and the number integral (NI) at  $r_{\min}$ . Note, the second number of the NI is given when the reverse coordination is different, and our simulation temperature was 473 K.

Peak	$r_{\max}$ / pm	$r_{\min}$ / pm	NI( $r_{\min}$ )
K-K (1.)	410	508	6.5
K-K (2.)	564	682	16.2
K-O	278	454	10.6/5.3
(OH <sup>-</sup> )		422	4.1/4.5
(H <sub>2</sub> O)		466	5.1/5.6
(H <sub>3</sub> O <sub>2</sub> <sup>-</sup> )		450	1.0/5.2
K...H	298	474	18.1/6.0
O...O	260	318	2.2
(OH)-(H <sub>2</sub> O)	259		1.8
(H <sub>2</sub> O)-(H <sub>2</sub> O)	282		0.5
O-H (1.)	98	128	1.5/1.0
O...H (2.)	160	240	2.7/1.8
H...H (1.)	162	185	0.8
H...H (2.)	208	292	3.5

mentioned above, proton transfers are prevalent, which means that the relative energy of this quasi-symmetrical structure is low, and therefore it can be seldom observed (4.3% of the time). This observation is fully supported by the unusually high  $g(r)$  value at the corresponding minimum (at 128 pm) of the O-H RDF (Figure 4 top right, orange), which in other, more dilute systems drops to almost zero. Table 2 also lists hydrogen bonds (160 pm) that appear to be contracted compared to a “normal” water hydrogen bond [29], and that may align with the compressed wire model of *Hassanali*. [23]

The solvation of water molecules also fundamentally differs from that known for pure water or dilute aqueous solutions. [29] In the latter systems, each water molecule donates most often two hydrogen bonds and accepts two more, giving a sum neighbor count of 4. However, in the present system water molecules have most often altogether hydrogen bonding 2 or 3 neighbors (43.7% and 27.8%, respectively), with neighbor counts of 0 (1.7%), 1 (16.1%), and 4 (8.7%) also present. The dissection of this data gives the average number of hydrogen bonds donated to a water molecule, which is surprisingly low (0.41), less than a quarter of that in pure water. The solvation of potassium ions is also very different from that reported earlier for dilute systems. In those cases, as mentioned above, the potassium has on average 6.5 neighboring oxygen atoms, [30, 31] while in our case, it was found to be 10.6. Interestingly, this number resembles that of the [6+4] coordination observed for the KOH·H<sub>2</sub>O crystal, [1] in which six O atoms are found in the range from 279 to 294 pm around the K atom, and four more between 327 and 362 pm (Figure 3). The larger distances in the simulations can be attributed to the dynamic rearrangement characteristic of the liquid phase, although K-O and K-K distances are, in general, very similar to those in the crystal phase. Interestingly, for NaOH solutions Hellström and Behler also found<sup>(10.1039/C6CP06547C)</sup> a slight increase of total coordination numbers at Na<sup>+</sup> ions in NaOH solutions as the concentration increased from dilute to

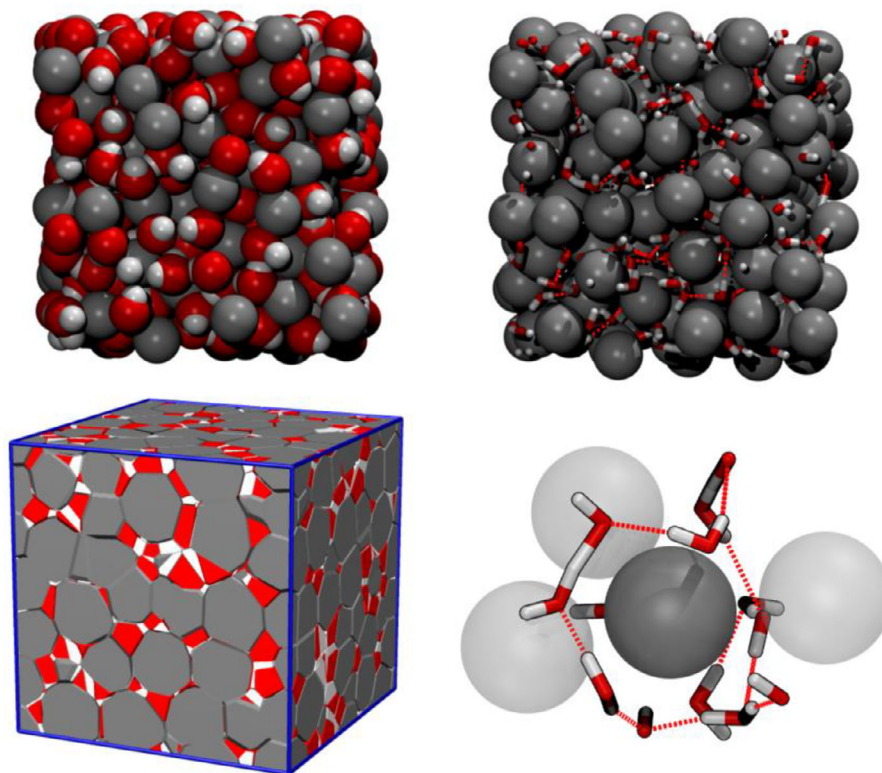


**FIGURE 5** | Visualization of the last simulation snapshot. Grey: K atom; Red: oxygen atom; White: Hydrogen atom. Upper left: van der Waals representation; upper right: K atoms as van der Waals representation and O as well as H atoms in Licorice representation. Lower left: The radical Voronoi cell of each atom of the system, colored white for hydrogen atoms, red for oxygen, and grey for potassium. Note, orientation above and below differs. Lower right: Arrangement of potassium cations separated by water molecules and hydroxide ions forming an extended hydrogen bonding network.

$x_{\text{NaOH}} = 0.3$ , although the changes—with the different cation in this more dilute solution—were much smaller than in the present case.

Considering the solvation of the three species, as described above, an unusual picture of the overall liquid hydroflux structure emerges. Some water molecules are not participating in the hydrogen bonding network, and their role is solely to coordinate the metal ion. The rest of the water molecules and hydroxide anions mostly form chains (coordination number 2) and sheets (coordination number 3) of hydrogen bonding assemblies, which clearly have termini (coordination number 1), and connections to other chains and sheets (coordination number 3 and 4). This low-dimensional hydrogen bonding network is also observable visually in the snapshot of the system in Figure 5.

In light of the literature discussions on proton transfer processes in acidic or basic aqueous media, this peculiar structure should have consequences also for the ability of the solution to exhibit structural diffusion. First, the hypercoordinated solvation of the hydroxide does not occur to any significant proportion, and therefore it cannot serve as a resting state for proton transfer processes. Related to this, the reduced proton transfer barriers further facilitate the process, as suggested by the relatively high minimum at 128 pm in the O–H RDF in Figure 4. Second, the reduced dimensionality of the hydrogen bonding network reduces the number of pathways, through which the transferred proton can return to its original location. However, this disruption may also reduce the prevalence of extended hydrogen-bond

chains (percolation pathways) necessary for long-range proton hopping. Thus, the increased preference of the hydroxide ion to accept a proton from the solution and the reduced barrier for the proton transfer itself, do not necessitate the presence of an actual effective Grotthuss diffusion in the system.

To quantify structural diffusion, we defined the oxygen atom partner of each hydrogen atom at each step of the simulation, to which it is covalently bound. When a proton transfer occurs, a change in this data can be observed. The subsequent proton transfers along a hydrogen bonding chain can be, therefore, defined, and the length of the chain along which the charge moves can be determined as well. Within this framework, we observed proton transfer events in unprecedented chain lengths involving up to seven oxygen atoms, which occurred not more than 1 ps within each other. Characterizing the prevalence of these chain events yields Figure 6 showing their probability within different time limits along different chain lengths. The data show that at least three oxygen atom hops occur within 1 ps of each other in 10% of the cases, whereas 0.4% of the proton transfers lead to chain events of length 6 or longer involving seven distinct oxygen atoms or more. This data clearly shows that there is a significant Grotthuss diffusion in the system.

### 3 | Conclusion

This study provides detailed evidence that water undergoes significant denaturation in highly concentrated mixtures with

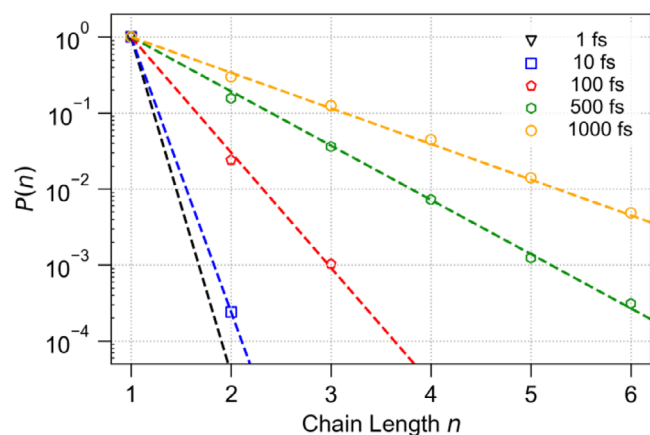


**FIGURE 6** | Cumulative percentage  $P(n)$  of proton transfer events that lead to a chain of  $n$  correlated proton transfers within a time frame of  $\tau = 1$  fs to 1000 fs between each individual proton transfer.

NaOH or KOH. Vapor pressure decreases and boiling points increase with increasing concentrations. A clear change in the slope of this correlation occurs at base concentrations  $c_B$  between 20 and 30 mol L<sup>-1</sup>, marking the transition from aqueous solutions — as used, for example, in hydrothermal syntheses and for electrolytes — to wet salt melts, known as hydroflux media. At molar water-base ratios of  $q(A) \leq 1$  ( $c_B \geq 55.5$  mol L<sup>-1</sup>), the water has a greatly reduced chemical activity and is essentially trapped in the melt by strong bonding interactions. Ab initio molecular-dynamics simulations reveal that the hydroxide and the water molecules form structural arrangements that differ from the solvation motives in more dilute or pure and ambient systems. Hydroxide ions are not found in a hypercoordinated structure, which hinders mobile protons to move, but are part of wire-like structures. Similarly, water does not assume the well-known fourfold coordination. These situations make the hydroflux system predestined for Grothuss diffusion, which we observe within 1 ps in wires with up to five oxygen atoms.

Overall, this combined experimental and computational analysis highlights the significant effect that ultra-alkaline conditions have on the macroscopic and microscopic properties of water. The results clearly demonstrate how extreme alkalinity disrupts traditional hydrogen bonding, alters vapor-liquid equilibria, and significantly affects molecular coordination and proton dynamics. These findings improve our understanding of how water behaves in alkaline salt melts, informing theoretical developments and practical applications in chemistry and materials science involving ultra-alkaline environments.

## Acknowledgments

This work was financially supported by the German Research Foundation (DFG, project-id: 438795198). The financial support for O.H. by the National Research, Development and Innovation Office through the project OTKA-FK 138823 is gratefully acknowledged. Furthermore, O.H. is grateful for the support from the János Bolyai Research Scholarship of the Hungarian Academy of Sciences. X. Z. is financially supported by the China Scholarship Council (CSC). B. K. and J. I. gratefully acknowledge the support

received from the FWO and F.R.S.-FNRS under the Excellence of Science programme (EOS 40007515) and the access to the Marvin cluster of the University of Bonn. B. K. thanks the DFG for their financial support under the CRC 1639 NuMerIQS (project-id: 511713970).

The authors thank Paul Zaby for providing access to refined AIMD trajectories.

Open access funding enabled and organized by Projekt DEAL.

## Conflicts of Interest

The authors declare no conflict of interest.

## References

- H. Jacobs, T. Tacke, and J. Kockelkorn, "Hydroxidmonohydrate des Kaliums und Rubidiums; Verbindungen, deren Atomanordnungen die Schreibweise  $K(H_2O)OH$  bzw.  $Rb(H_2O)OH$  nahelegen," *Zeitschrift für Anorganische und Allgemeine Chemie* 516 (1984): 67.
- D. Elwell and H. J. Scheel, *Crystal Growth From High-Temperature Solutions* (London (England): Academic Press Inc), (1975).
- G. J. Harms and W. Gunßer, "Wet Salt Melts — A Reaction Medium Suitable for the Preparation of Metastable Oxides and Hydroxides?" *Berichte der Bunsengesellschaft für physikalische Chemie* 90 (1986): 764.
- W. M. Chance, PhD Thesis, University of South Carolina (USA), (2014).
- D. E. Bugaris, M. D. Smith, and H.-C. zur Loye, "Hydroflux Crystal Growth of Platinum Group Metal Hydroxides:  $Sr_6NaPd_2(OH)_{17}$ ,  $Li_2Pt(OH)_6$ ,  $Na_2Pt(OH)_6$ ,  $Sr_2Pt(OH)_8$ , and  $Ba_2Pt(OH)_8$ ," *Inorganic Chemistry* 52 (2013): 3836.
- W. M. Chance, D. E. Bugaris, A. S. Sefat, and H.-C. zur Loye, "Crystal Growth of New Hexahydroxometallates Using a Hydroflux," *Inorganic Chemistry* 52 (2013): 11723.
- A. M. Latshaw, W. M. Chance, G. Morrison, et al., "Synthesis of a Ferrolite: A Zeolitic all-Iron Framework," *Angewandte Chemie International Edition* 55 (2016): 13195.
- T. K. Deason, M. A. Grasser, A. M. Mofrad, et al., "Ionothermal Synthesis of  $Am_4B_{22}O_{42}Cl_{12}$ : A Chiral Cubic Americium Borate Cluster," *Inorganic Chemistry* 64 (2025): 2182.
- R. Albrecht, PhD Thesis, Technische Universität Dresden (Germany), (2022).
- R. Albrecht, H. Poddig, J. Hunger, et al., "Hydrothermal Synthesis, Crystal Structure, and Magnetism of  $Na_2[Ir(OH)_6]$  and Its Dehydration to  $Na_2IrO_3$ ," *Zeitschrift für Anorganische und Allgemeine Chemie* 647 (2021): 667.
- R. Albrecht and M. Ruck, "Chalcogenides by Reduction of Their Dioxides in Ultra-Alkaline Media," *Angewandte Chemie International Edition* 60 (2021): 22570.
- Y. Li, P. A. Hegarty, M. Rüsing, L. M. Eng, and M. Ruck, "Ba(BO<sub>2</sub>OH) — A Monoprotonated Monoborate From Hydroflux Showing Intense Second Harmonic Generation," *Zeitschrift für Anorganische und Allgemeine Chemie* 648 (2022): e202200193.
- H. He, R. Albrecht, and M. Ruck, "Orthoperiodato Rhodium(III) Complex as a Possible Key to Catalytic Oxidation of Organic Dyes," *Zeitschrift für Anorganische und Allgemeine Chemie* 648 (2022): e202200041.
- C. V. M. Inocêncio, A. Torres-Pardo, D. Montero, et al., "Crystallization of Manganese(V) Oxides by Hydroflux Synthesis: Control of Anisotropic Growth and Electrochemical Stability," *Inorganic Chemistry* 64 (2025): 5122.

15. A. G. Iwanicki, B. Wilfong, E. Zoghlin, W. Bunstine, M. A. Siegler, and T. M. McQueen, "Hydroflux-controlled Growth of Magnetic K-Cu-Te-O(H) Phases," *Physical Review Materials* 8 (2024): 114423.
16. D. Badae, S. Olthof, J. M. Neudörfl, et al., "K<sub>3</sub>[MO<sub>4</sub>][MO<sub>3</sub>N] (M = Tc, Re)—Nitridotrioxidorhenate and -technetate From Highly Alkaline Media" *European Journal of Inorganic Chemistry* (2023): 26, e202300481.
17. X. Zhou, B. Wilfong, X. Chen, et al., "Sr(Ag<sub>1-x</sub>Li<sub>x</sub>)<sub>2</sub>Se<sub>2</sub> and [Sr<sub>3</sub>Se<sub>2</sub>][(Ag<sub>1-x</sub>Li<sub>x</sub>)<sub>2</sub>Se<sub>2</sub>] Tunable Direct Band Gap Semiconductors" *Angewandte Chemie International Edition* (2023): 62, e202301191.
18. M. Chen, L. Zheng, B. Santra, et al., "Hydroxide Diffuses Slower Than Hydronium in Water Because Its Solvated Structure Inhibits Correlated Proton Transfer," *Nature Chemistry* 10 (2018): 413.
19. S. Dasgupta, G. Cassone, and F. Paesani, "Nuclear Quantum Effects and the Grothuss Mechanism Dictate the pH of Liquid Water," *Journal of Physical Chemistry Letters* 16 (2025): 2996.
20. B. Kirchner, "Eigen or Zundel Ion: News From Calculated and Experimental Photoelectron Spectroscopy" *ChemPhysChem* (2007): 8, 41.
21. M. E. Tuckerman, D. Marx, and M. Parrinello, "The Nature and Transport Mechanism of Hydrated Hydroxide Ions in Aqueous Solution," *Nature* 417 (2002): 925.
22. P. B. Calio, C. Li, and G. A. Voth, "Resolving the Structural Debate for the Hydrated Excess Proton in Water," *Journal of the American Chemical Society* 143 (2021): 18672.
23. A. Hassanal, M. K. Prakash, H. Eshet, and M. Parrinello, "On the Recombination of Hydronium and Hydroxide Ions in Water," *PNAS* 108 (2011): 20410.
24. N. Agmon, "The Grothuss Mechanism," *Chemical Physics Letters* 244 (1995): 456.
25. J. Balej, "Water Vapor Partial Pressures and Water Activities in Potassium and Sodium Hydroxide Solutions Over Wide Concentration and Temperature Ranges," *International Journal of Hydrogen Energy* 10 (1985): 233.
26. P. Stange, K. Fumino, and R. Ludwig, "Ion Speciation of Protic Ionic Liquids in Water: Transition From Contact to Solvent-Separated Ion Pairs," *Angewandte Chemie International Edition* 52 (2013): 2990.
27. P. Habibi, A. Rahbari, S. Blazquez, et al., "A New Force Field for OH<sup>-</sup> for Computing Thermodynamic and Transport Properties of H<sub>2</sub> and O<sub>2</sub> in Aqueous NaOH and KOH Solutions," *Journal of Physical Chemistry B* 126 (2022): 9376.
28. Z. Yin, P. Krasnov, S. Thürmer, et al., "Observation of an Associative State in Aqueous Hydroxide," *Journal of the American Chemical Society* 147 (2025): 9190.
29. R. Ludwig, "Water: From Clusters to the Bulk," *Angewandte Chemie International Edition* 40 (2001): 1808.
30. C. N. Rowley and B. Roux, "The Solvation Structure of Na<sup>+</sup> and K<sup>+</sup> in Liquid Water Determined From High Level Ab Initio Molecular Dynamics Simulations" *Journal of Chemical Theory and Computation* (2012): 8, 3526.
31. Y. Liu, H. Lu, Y. Wu, T. Hu, and Q. Li, "Hydration and Coordination of K<sup>+</sup> Solvation in Water From Ab Initio Molecular-dynamics Simulation" *Journal of Chemical Physics* (2010): 132, 124503.
32. L. Martínez, L. Martínez, R. Andrade, E. G. Birgin, and J. M. Martínez, "PACKMOL: A Package for Building Initial Configurations for Molecular Dynamics Simulations," *Journal of Computational Chemistry* 30 (2009): 2157.
33. W. L. Jorgensen, D. S. Maxwell, and J. Tirado-Rives, "Development and Testing of the OPLS all-atom Force Field on Conformational Energetics and Properties of Organic Liquids," *Journal of the American Chemical Society* 118 (1996): 11225.
34. H. J. C. Berendsen, J. R. Grigera, and T. P. Straatsma, "The Missing Term in Effective Pair Potentials," *Journal of Physical Chemistry* 91 (1987): 6269.
35. T. D. Kühne, M. Iannuzzi, M. Del Ben, et al., "CP2K: An Electronic Structure and Molecular Dynamics Software Package — Quickstep: Efficient and Accurate Electronic Structure Calculations" *Journal of Chemical Physics* (2020): 152, 194103.
36. J. VandeVondele, M. Krack, F. Mohamed, M. Parrinello, T. Chassaing, and J. Hutter, "Quickstep: Fast and Accurate Density Functional Calculations Using a Mixed Gaussian and Plane Waves Approach," *Computer Physics Communications* 167 (2005): 103.
37. J. VandeVondele and J. Hutter, "Gaussian Basis Sets for Accurate Calculations on Molecular Systems in Gas and Condensed Phases," *Journal of Chemical Physics* 127 (2007): 114105.
38. M. Krack, "Pseudopotentials for H to Kr Optimized for Gradient-corrected Exchange-correlation Functionals," *Theoretical Chemistry Accounts* 114 (2005): 145.
39. C. Hartwigsen, S. Goedecker, and J. Hutter, "Relativistic Separable Dual-Space Gaussian Pseudopotentials From H to Rn," *Physical Review B* 58 (1998): 3641.
40. S. Goedecker, M. Teter, and J. Hutter, "Separable Dual-Space Gaussian Pseudopotentials," *Physical Review B* 54 (1996): 1703.
41. S. Grimme, S. Ehrlich, and L. Goerigk, "Effect of the Damping Function in Dispersion Corrected Density Functional Theory," *Journal of Computational Chemistry* 32 (2011): 1456.
42. S. Grimme, J. Antony, S. Ehrlich, and H. Krieg, "A Consistent and Accurate Ab Initio Parametrization of Density Functional Dispersion Correction (DFT-D) for the 94 Elements H–Pu" *Journal of Chemical Physics* (2010): 132.
43. W. G. Hoover, H. A. Posch, B. L. Holian, M. J. Gillan, M. Mareschal, and C. Massobrio, "Dissipative Irreversibility From Nosé's Reversible Mechanics" *Molecular Simulation* (1987): 1, 79.
44. S. Nosé, "Constant-temperature Molecular Dynamics," *Journal of Physics-Condensed Matter* 2 (1990): SA115.
45. M. Brehm, M. Thomas, S. Gehrke, and B. Kirchner, "TRAVIS—A Free Analyzer for Trajectories From Molecular Simulation" *Journal of Chemical Physics* (2020): 152.
46. M. Brehm and B. Kirchner, "TRAVIS—A Free Analyzer and Visualizer for Monte Carlo and Molecular Dynamics Trajectories" *Journal of Chemical Information and Modeling* (2011): 51, 2007.
47. O. C. Bridgeman and E. W. Aldrich, "Vapor Pressure Tables for Water," *Journal of Heat Transfer* 86 (1964): 279.

### Supporting Information

Additional supporting information can be found online in the Supporting Information section.

The Supporting Information provides details and additional data about the device, the pressure measurement methodology, and the AIMD simulations. The authors have cited additional references within the Supporting Information [32–47]. **Supporting file 1:** chem70521-sup-0001-SuppMat.pdf